

# Follow-up of zirconia crystallization on a surface modified alumina powder

V. Naglieri<sup>a,b</sup>, L. Joly-Pottuz<sup>b</sup>, J. Chevalier<sup>b,\*</sup>, M. Lombardi<sup>a</sup>, L. Montanaro<sup>a</sup>

<sup>a</sup> Dept. Mater. Sci. and Chem. Eng., INSTM LINCE Lab., Politecnico di Torino, Corso Duca degli Abruzzi 24, 10129 Torino, Italy

<sup>b</sup> Université de Lyon, INSA de Lyon, MATEIS UMR CNRS 5510, Bât. Blaise Pascal, 7 Av. Jean Capelle, 69621 Villeurbanne, France

Received 18 February 2010; received in revised form 4 July 2010; accepted 16 July 2010

Available online 19 August 2010

## Abstract

Here we report how thermal treatments of a surface modified  $\alpha$ -alumina powder on which a zirconium oxide precursor was grafted can be tailored so as to obtain an alumina–zirconia composite powder with well-controlled phase distribution and size. The transformation of the zirconia precursor from a starting amorphous phase to zirconia nano-grains bonded to the alumina particles surface was followed by X-ray diffraction (performed at room temperature on different thermally treated powders, as well as *in situ* at high-temperature) and by both conventional and high resolution transmission electron microscopy (TEM and HRTEM). Phase and nanostructure evolutions were followed on a large temperature span. The crystallization kinetics were analysed in terms of nucleation–growth mechanisms by exploiting Avrami–Johnson–Mehl–Kolmogorov formalism. Based on the above investigations, a tentative description of nucleation and growth features is proposed. This knowledge-based step represents a first approach towards nanopowders engineering.

© 2010 Elsevier Ltd. All rights reserved.

**Keywords:** Calcination; Sintering; Grain growth; Nanocomposites; Microstructure-final; Microstructure-prefiring

## 1. Introduction

Alumina–zirconia composites are used as grinding media and cutting-tools, wear parts<sup>1</sup> and biomedical implants,<sup>2,3</sup> since they exhibit high hardness, strength and high fracture toughness due to transformation toughening mechanisms.<sup>4–7</sup> Especially, they are raising interest in orthopaedics, since they exhibit a larger crack resistance than alumina and a lower sensitivity to aging than zirconia. However, the content and the distribution of zirconia grains inside the alumina matrix have a strong impact on their performances.<sup>2</sup> In particular, micro-nano-composites in which nano-zirconia particles are embedded in micron sized alumina matrix are expected to exhibit improved slow crack growth resistance and stability.<sup>8</sup> To achieve the control of microstructural features at different scales, each step of the process, from powder synthesis to sintering, must be carefully set up.

Alumina–zirconia powders can be prepared by various strategies, from the simple powder-mixing<sup>2</sup> to chemically based routes, like sol–gel,<sup>4,9,10</sup> co-precipitation,<sup>11</sup> and mixed-salts thermal decomposition.<sup>12,13</sup> Torrecillas and co-workers recently

proposed a sophisticated and effective approach based on the powder–alkoxide mixture,<sup>14</sup> in which a zirconium alkoxide is grafted to the surface of alumina grains. After thermal treatments, zirconia nanocrystals, strongly bonded to the alumina surface, are developed. Such promising route has been applied and simplified by working in aqueous medium with inorganic zirconium salts.<sup>15</sup> These powders offer the opportunity to develop dense composite materials with very fine and homogeneous microstructures, which represent a robust approach towards real nanostructured ceramic materials with promising properties. However, to our knowledge, there is still a lack of investigation concerning the intermediate steps between the starting amorphous phase on the alumina surface and the final developed microstructure, whereas a strict control of the nucleation and growth of zirconia crystals is needed to really achieve fully tailored microstructures.

Here, this aim was pursued, by a precise follow-up of zirconia crystallization at the surface of alpha alumina grains during thermal treatments via X-ray diffraction (XRD) analysis and TEM observations. The final goal of the present work was to propose a possible nucleation–growth scenario able to support the choice of a suitable powder treatment to tailor phase distribution and size in the alumina–zirconia composite powder and consequently on sintered bodies.

\* Corresponding author.

E-mail address: [jerome.chevalier@insa-lyon.fr](mailto:jerome.chevalier@insa-lyon.fr) (J. Chevalier).

## 2. Materials and methods

### 2.1. Powder preparation

Surface modification of a commercial  $\alpha$ -alumina powder (TM-DAR TAIMICRON, Taimei Chemical Co., Japan.) was carried out to finally obtain a 95 vol% alumina–5 vol% zirconia composite powder. The procedure has been already described elsewhere.<sup>15</sup> Briefly, a zirconium chloride aqueous solution is first prepared, adding tribasic ammonium citrate to get a pH value of about 4, and added under stirring to a well dispersed aqueous alumina suspension. Spray drying (Mini Spray Drier Buchi B-290) is finally performed (inlet temperature of 140 °C) to produce a starting surface modified powder, avoiding any salt segregation.

### 2.2. Crystallization process

#### 2.2.1. In situ follow-up

The behavior of the powder was followed *in situ* by two methods:

- Simultaneous thermo gravimetric analysis – differential thermal analysis (TGA–DTA, SETARAM TG-DTA 92, Caluire, France) were carried out on 115 mg of powder, heated in 20% N<sub>2</sub>–80% O<sub>2</sub> atmosphere at 5 °C min<sup>-1</sup> up to 1000 °C.
- High-temperature-XRD analyses were performed *in situ*, on a Bruker diffractometer (Cu anticathode,  $\lambda_{\text{Cu}}$  1.54060 Å,  $2\theta$  range 24.2–38.3°) equipped with a furnace allowing the samples to be heated up to 1200 °C. Two kinds of experiments were carried out:
  - (i) *Isochronal treatments*: Heating the sample from room temperature up to 1000 °C (temperature ramps of 1.5 °C min<sup>-1</sup>, 4.2 °C min<sup>-1</sup>, 5.6 °C min<sup>-1</sup>, 30 °C min<sup>-1</sup> respectively);
  - (ii) *Isothermal treatments*: Heating the sample (temperature ramp of 30 °C min<sup>-1</sup>, i.e. the maximum heating rate allowed by the apparatus) up to 500 °C, 600 °C, 800 °C, 1000 °C or 1200 °C, respectively, followed by an isotherm at the maximum temperature for 12 h.

#### 2.2.2. Characterization of thermally treated powders

The phase evolution was investigated after several thermal treatments (heating and cooling rate = 10 °C min<sup>-1</sup>) up to the following temperatures: 500 °C, 600 °C, 800 °C and 1000 °C, for a soaking time at the maximum temperature of 1 h and 10 h, respectively. Small samples of powder were also submitted to isothermal treatments, by quickly plunging them into a furnace already at a steady temperature (i.e. 500 °C, 600 °C, 800 °C, 1000 °C, respectively), holding them in temperature for duration ranging from 1 min to 24 h and then quenching in ambient air.

The following characterization tests were then performed:

- Conventional XRD analyses (XRD, Philips PW 1710, Cu anticathode,  $\lambda_{\text{Cu}}$  1.54060 Å,  $2\theta$  range 24–33°) were carried out on isothermally treated samples. The average crystallite size was calculated by the line-broadening method, using the

Scherrer's equation:

$$D = \frac{k \cdot \lambda}{\beta \cdot \cos \theta} \quad (1)$$

where  $D$  is the crystallite size,  $\lambda$  is the wavelength of the CuK $\alpha$  line (1.54060 Å),  $k$  is the Scherrer constant equal to 0.9, and  $\beta$  is the full width at half maximum of the main zirconia peak ( $2\theta \cong 30.25^\circ$ ), corrected by the experimental width of the apparatus and assuming a Gaussian profile.

The area of the main zirconia peak (1 0 1)<sub>t</sub> was measured and used to calculate a crystalline degree index: the crystalline fraction  $f$  of each sample was calculated as the ratio between the area of its main zirconia peak and that presented by a sample in which zirconia was fully crystallized.

- TEM (LEO 912 instrument, operating at 120 kV accelerating voltage) on powders after thermal treatments was used to observe the appearance and growth of zirconia crystallites on alumina grains surface. Specimens were prepared by slow evaporation of a drop of the powder suspension in ethanol, deposited onto a perforated carbon-covered copper grid. Images were collected both in bright field (BF, Fig. 1a) and dark field (DF, Fig. 1b) mode. In the latter case, images were obtained with the objective aperture positioned on the first zirconia ring of the diffraction pattern (Fig. 1c), at which the objective aperture only selects the electrons which are in Bragg conditions for zirconia crystallites, so that only zirconia crystallites are illuminated as white dots. Furthermore, we used a specific feature available on LEO microscope that allows performing annular dark field (ADF) images in the TEM mode. This is made possible by rotating the diffraction pattern through the small objective aperture so that the whole selected ring is used to give the DF image. Thus all the zirconia crystallites in Bragg conditions can be imaged in the sample, allowing a more precise determination of their size distribution through numerical analyses performed on DF low magnification images. For each thermal treatment, more than 600 zirconia crystallites were measured, in order to monitor the evolution of the mean zirconia crystallites size as a function of treatment temperature and time.
- High resolution transmission electron microscopy (HRTEM) was also performed on selected thermally treated powders on JEOL 2010 F Microscope under 200 kV Voltage.
- The phase evolution was also followed by Raman spectroscopy (Labram HR 800 microspectrometer manufactured by Jobin Yvon), performed on the samples *in situ* heat-treated in the HT-XR Diffractometer. A 50× microscope objective lens was used for focusing the laser beam and collecting the scattered light. An excitation wavelength of 514.5 nm was produced by an argon laser source. The instrumental resolution was 1 cm<sup>-1</sup> for the 1800 g/mm grating. The calibration was performed with silicon semiconductor at 520.7 cm<sup>-1</sup>. All peaks were deconvoluted by using a Lorentzian fitting.<sup>16</sup>

### 2.3. Final microstructure in sintered samples

In order to investigate the influence of the powder thermal treatment on the final microstructure, two composite powders,

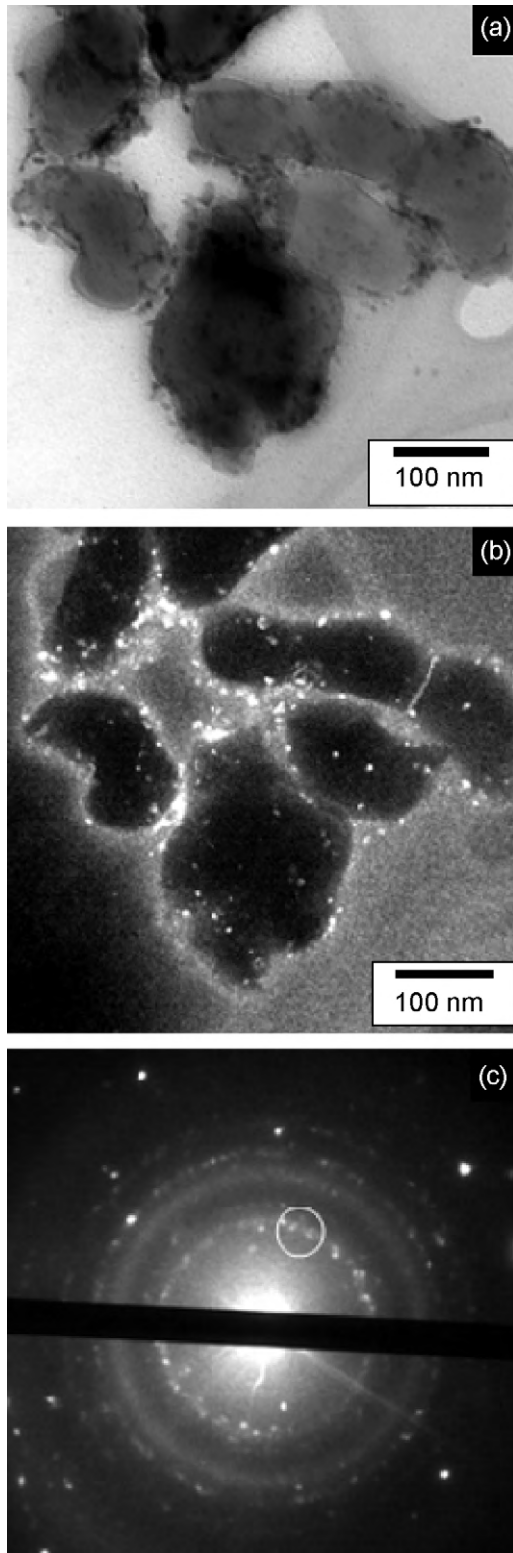


Fig. 1. TEM images of the 95 vol% alumina–5 vol% zirconia powder after treatment at 500 °C for 1 h: (a) bright field image, (b) dark field image obtained with the objective aperture on one ring of zirconia structure as shown by the circle on the respective diffraction pattern (c).

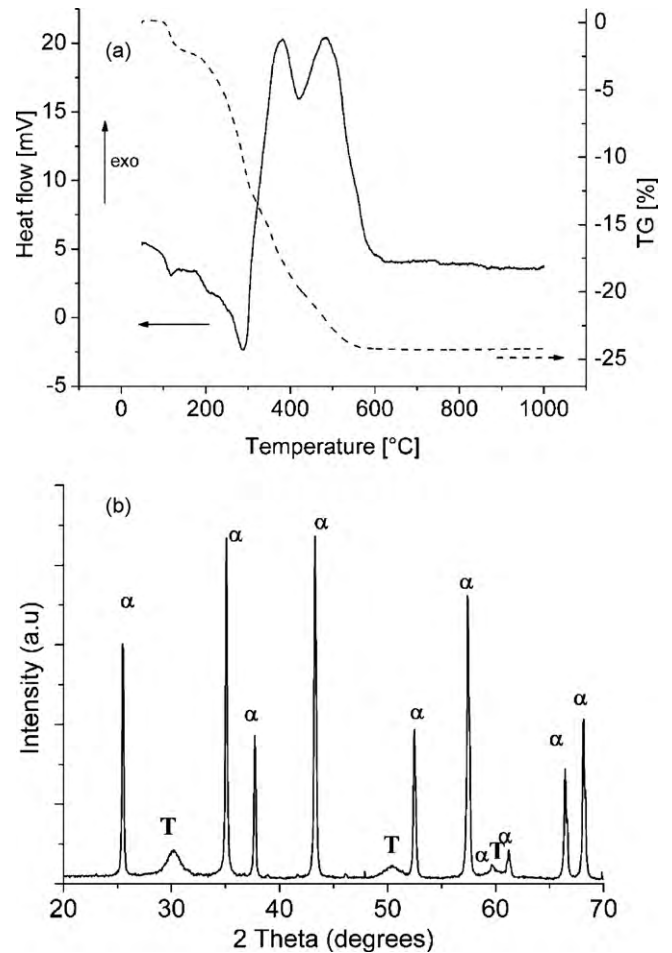


Fig. 2. (a) DTA (solid line) and TGA (dashed line) curves of the as-dried 95 vol% alumina–5 vol% zirconia powder, and (b) XRD pattern of the powder treated at 500 °C for 1 h (heating rate of 10 °C min<sup>-1</sup>, T=tetragonal zirconia, α = alpha alumina).

treated at 600 °C for 1 h and 10 h, respectively, were used to produce samples by slip casting. For this purpose, the composite powders were dispersed by ball milling in water at pH 4.5 with a solid content of 60 wt.% and the suspensions were poured into porous moulds. These conditions have been proven previously to give satisfactory dispersion.<sup>2</sup> The green bodies were dried in a humidity-controlled chamber, and finally sintered at 1500 °C for 3 h, which represents a standard heat treatment for such composites.<sup>2</sup> The fired microstructures were submitted to SEM characterization (ESEM XL 30, FEI, The Netherlands), performed on polished and thermally etched surfaces.

### 3. Results

#### 3.1. Organic by-products decomposition and zirconia crystallization start

From TGA–DTA curve (Fig. 2a), the total mass loss of about 24% was completely recorded in the 100–600 °C temperature range, imputable to by-products (such as ammonium citrate and chloride) thermal decomposition. The exothermic peaks, between 300 °C and 600 °C, are given by several overlapped phe-

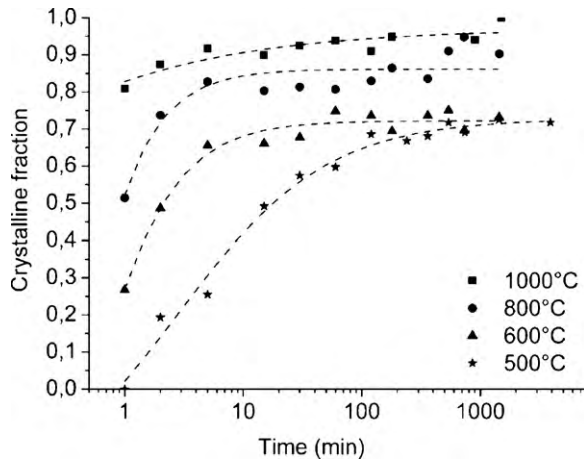


Fig. 3. Zirconia crystalline fraction vs. time, in 95 vol% alumina–5 vol% zirconia powder, submitted to isothermal treatments in furnace at different temperatures.

nomena, such as decarboxylation, organic skeleton destruction, carbon burning, chloride release,<sup>17</sup> and also zirconia crystallization into tetragonal phase, as supported by X-ray diffraction analysis performed on the powder calcined at 500 °C for 1 h (Fig. 2b).

### 3.2. Crystalline fraction evolution during isothermal treatments

Fig. 3 shows the crystalline fraction vs. time, measured on samples isothermally treated in the temperature range 500–1000 °C. The crystallization rate increases with the increase of the treatment temperature. The crystallized fraction after 1 min is about zero for the powder treated at 500 °C, and about 26%, 51% and 80% for the samples treated at 600 °C, 800 °C and 1000 °C, respectively. It was not possible to evaluate an induction time for crystallization, except in the case of the isotherm at 500 °C, since in this case crystalline zirconia is not detectable after 1 min, but a crystalline degree of about 20% is reached just after 2 min.

The crystallization kinetics were analysed using the Avrami equation,<sup>18</sup> for isothermal heating:

$$f = 1 - \exp(-(Kt)^n) \quad (2)$$

where  $f$  is the crystalline volume fraction obtained by the isothermal treatment for the time  $t$ ,  $K$  is a rate constant, and  $n$  is the Avrami exponent. The Avrami exponent can be determined from the logarithmic form of the previous equation:

$$\ln \left( \ln \left( \frac{1}{1-f} \right) \right) = n \cdot \ln(K) + n \cdot \ln(t) \quad (3)$$

The rate constant  $K$  can be expressed in the form of an Arrhenius equation:

$$K = K_0 \cdot \left( \frac{-Q}{RT} \right) \quad (4)$$

Thus the relation between  $\ln K$  and  $1/T$  should be linear and the slope of the straight line is the apparent activation energy,  $Q$ .

Table 1

Avrami exponents obtained from isothermal and isochronal treatments at different temperatures and for different heating rates.

Temperature (°C)	Avrami exponent
Isothermal treatments	
500	0.16
600	0.05
800	0.09
1000	0.13
Isochronal treatments	
450	0.41
550	0.17
750	0.18
950	0.09

The calculated Avrami exponents for isothermal treatments are in the range of 0.05–0.16 (see numerical values in Table 1), while the apparent activation energy  $Q$  is 131 kJ mol<sup>-1</sup>.

### 3.3. Crystalline fraction evolution during isochronal treatments

In view of a more precise follow-up of zirconia crystallization, based on a large data amount collected by carrying out faster experiments, *in situ* HT-XRD analyses were performed. Since a real isothermal treatment cannot be achieved in a diffractometer, zirconia crystallization was monitored under a constant heating rate. In fact, the Avrami exponent can be calculated also using non-isothermal methods, when the heating rate is kept constant, just modifying the Eq. (3) as follows:<sup>19</sup>

$$\ln \left( \ln \left( \frac{1}{1-f} \right) \right) = n \cdot \ln(K) - n \cdot \ln(v) \quad (5)$$

where  $v$  is the heating rate, and  $f$  is the crystallized fraction as determined by the area of the main zirconia XRD peak. In these experiments the phase evolution was followed in samples treated at several heating rates, kept constant during each experiment. Fig. 4 plots the trend of the crystalline fraction vs. temperature, for the different heating rates. The crystallization rate increases

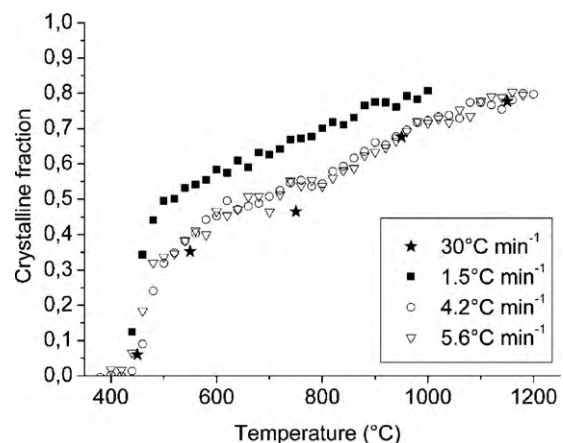


Fig. 4. Zirconia crystalline fraction vs. temperature, in 95 vol% alumina–5 vol% zirconia powder *in situ* treated in HT-XRD, at different heating rates.

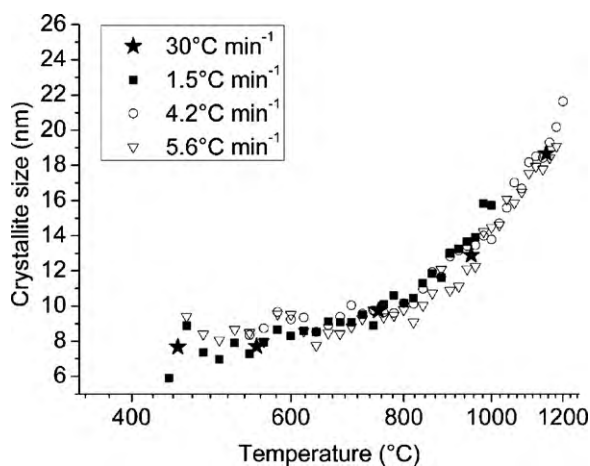


Fig. 5. Zirconia crystallite size vs. time for 95 vol% alumina–5 vol% zirconia powder (isochronal treatments in HT-XRD).

as the heating rate decreases, and the calculated Avrami exponents are in the range 0.09–0.41 (Table 1), while the apparent activation energy  $Q$  is  $111 \text{ kJ mol}^{-1}$ .

The Avrami exponents, calculated by exploiting both the isothermal and isochronal methods, are comparable and in agreement with the data reported by Ghosh et al.,<sup>20</sup> that is a low Avrami exponent (0.45) for the primary crystallization of  $\text{ZrO}_2$ –3mol%  $\text{Y}_2\text{O}_3$  in the temperature range of 500–575 °C.

### 3.4. Crystallite size evolution

The mean crystallite size evolution was first followed as a function of temperature during isochronal treatments (Fig. 5). The growth rate is roughly independent of the heating rate, in the investigated range ( $1.5$ – $30 \text{ °C min}^{-1}$ ), but strongly affected by the temperature. Below 800 °C, crystallite size remains almost constant (roughly 8–10 nm), whereas it varies from 10 nm to more than 21 nm in the temperature range 800–1200 °C. This trend is confirmed by the evolution of the crystallite size vs. time during the isothermal treatments (Fig. 6a and b): the growth rate is apparently close to zero below 800 °C, while the treatment time starts to play a role in crystallite growth at 1000 °C.

The differences in size, observed by comparing the data from the two methods (i.e. isothermal treatments in the furnace or in the HT-XRD), are reasonably imputable to the different real temperature of the samples. Anyway, the trends are in good agreement.

For the powders isothermally treated in HT-XRD, the zirconia crystallites are about 8 nm in size at 500 °C, and they grow up to 32 nm after 12 h at 1200 °C; however, phase transformation from tetragonal to monoclinic zirconia was not observed, even if no stabilizer (i.e. no yttria) was present. An activation energy for crystallite growth of  $43 \text{ kJ mol}^{-1}$  was calculated from the large number of available data collected by HT-XRD. It is in agreement with literature data, related to the growth activation energy of nanocrystalline grains.<sup>20,21</sup> In those papers, a lower activation energy for nanocrystalline growth, with respect to the value for bulk materials, was imputed to the grain-rotation-induced grain coalescence mechanism, possible in free-standing powder.<sup>20,21</sup>

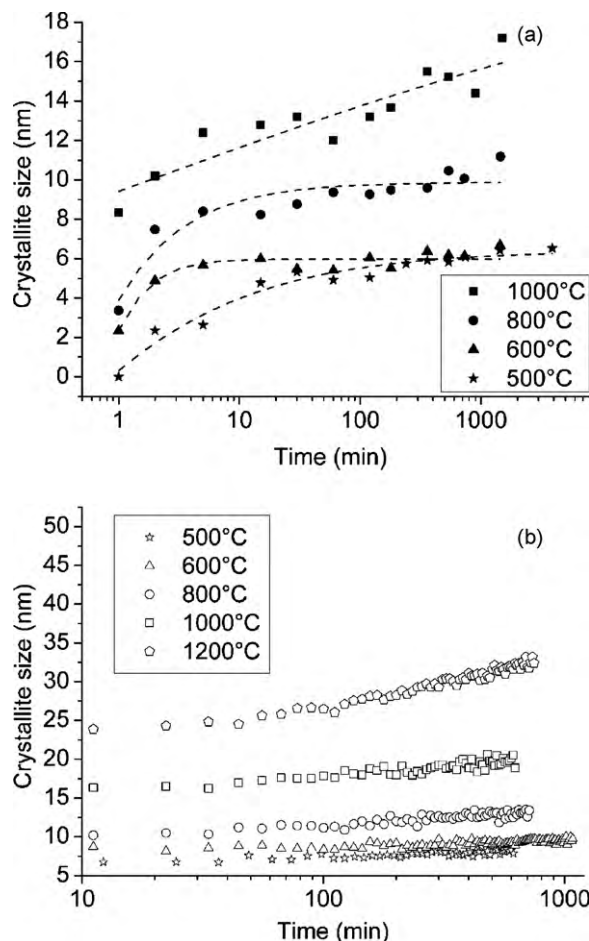


Fig. 6. Zirconia crystallite size vs. time for isothermal treatments in furnace (a) and in HT-XRD (b) for 95 vol% alumina–5 vol% zirconia powder.

### 3.5. Additional information by TEM, HRTEM and Raman spectroscopy

The zirconia crystallites formation was followed by TEM observations. Fig. 7 shows TEM images of samples submitted to different heat treatments. After calcination at 500 °C for 1 h, alumina grains are surrounded by an amorphous layer (Fig. 7a). Small zirconia crystallites are observable inside the amorphous phase, almost completely detached from the alumina surfaces. After 10 h at 500 °C, zirconia crystallites grow and partially aggregate (Fig. 7b). After treatment at 600 °C, a lower amount of amorphous phase is detected all around the alumina grains (Fig. 7c) and, prolonging the treatment, a similar trend than at 500 °C is observed: discrete amorphous phase pockets appear in which crystallites tend to agglomerate (Fig. 7d). Finally, treatments at 800 °C and 1000 °C led to the progressive crystallite growth (Fig. 7e and g). These observations strengthened the previous results: the treatment duration seems to have a poor influence on crystallite growth at the lower treatment temperatures. In addition, due to their low affinity to the alumina grains surface, the small zirconia crystallites are drained by the amorphous phase flow into discrete pockets in which they can start to aggregate. This is of primary importance since aggregation could lead to coalescence and growth of the zirconia grains dur-

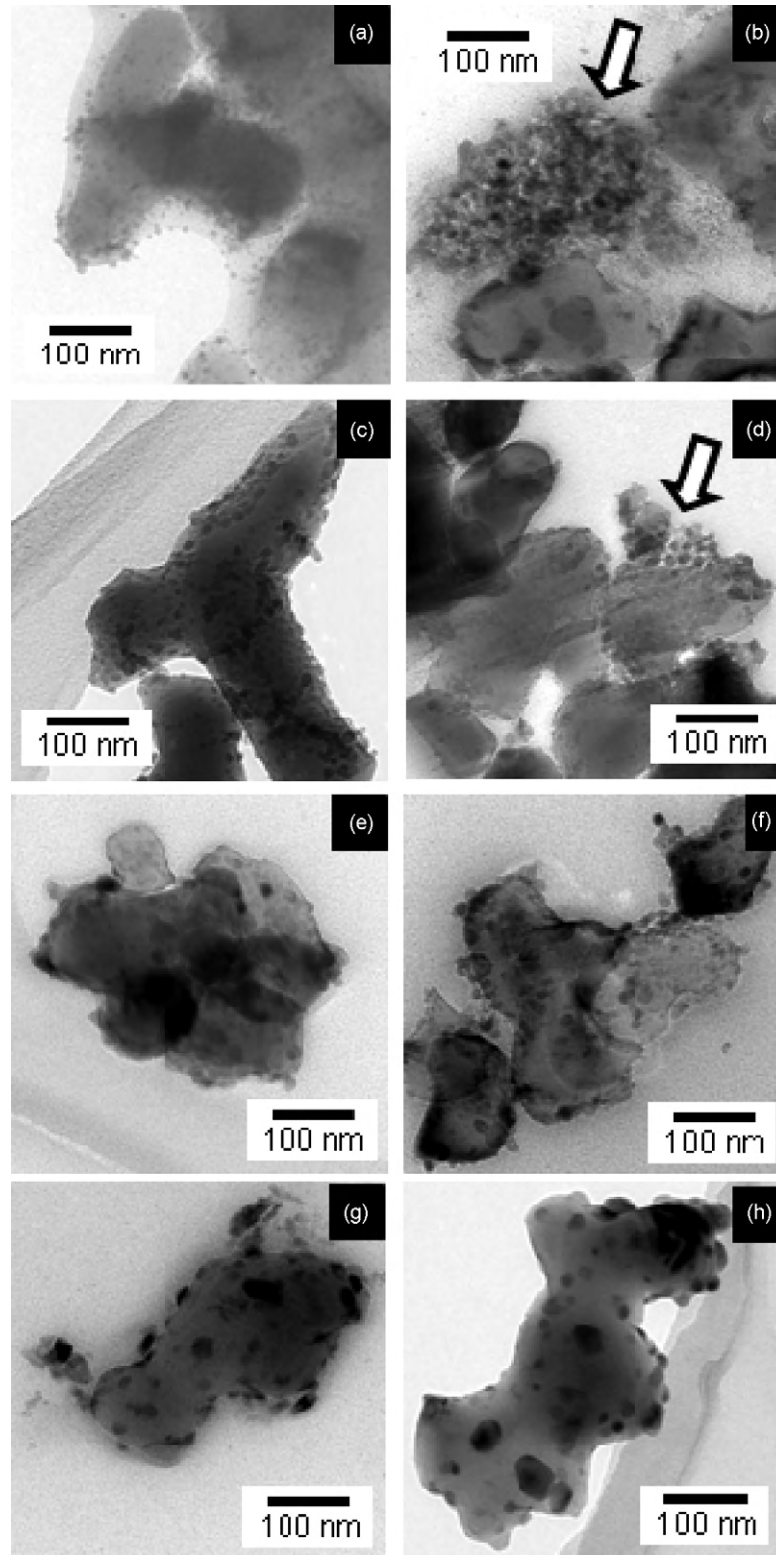


Fig. 7. BF TEM images of 95 vol% alumina–5 vol% zirconia powder after treatments at different temperatures and times: (a) 500 °C – 1 h, (b) 500 °C – 10 h, (c) 600 °C – 1 h, (d) 600 °C – 10 h, (e) 800 °C – 1 h, (f) 800 °C – 10 h, (g) 1000 °C – 1 h, (h) 1000 °C – 10 h. The arrows indicate the zirconia nuclei drained into discrete pockets.

ing sintering, hindering the microstructural control as well as the preservation of the nanostructure.

HRTEM was also performed for a deeper understanding of zirconia crystallization process. In Fig. 8 a detail of the amor-

phous phase surrounding an alumina grain after calcination at 500 °C for 1 h is presented: nano-sized zirconia crystallites are dispersed in the amorphous phase and only occasionally they are in contact with the alumina grains surface. These observa-

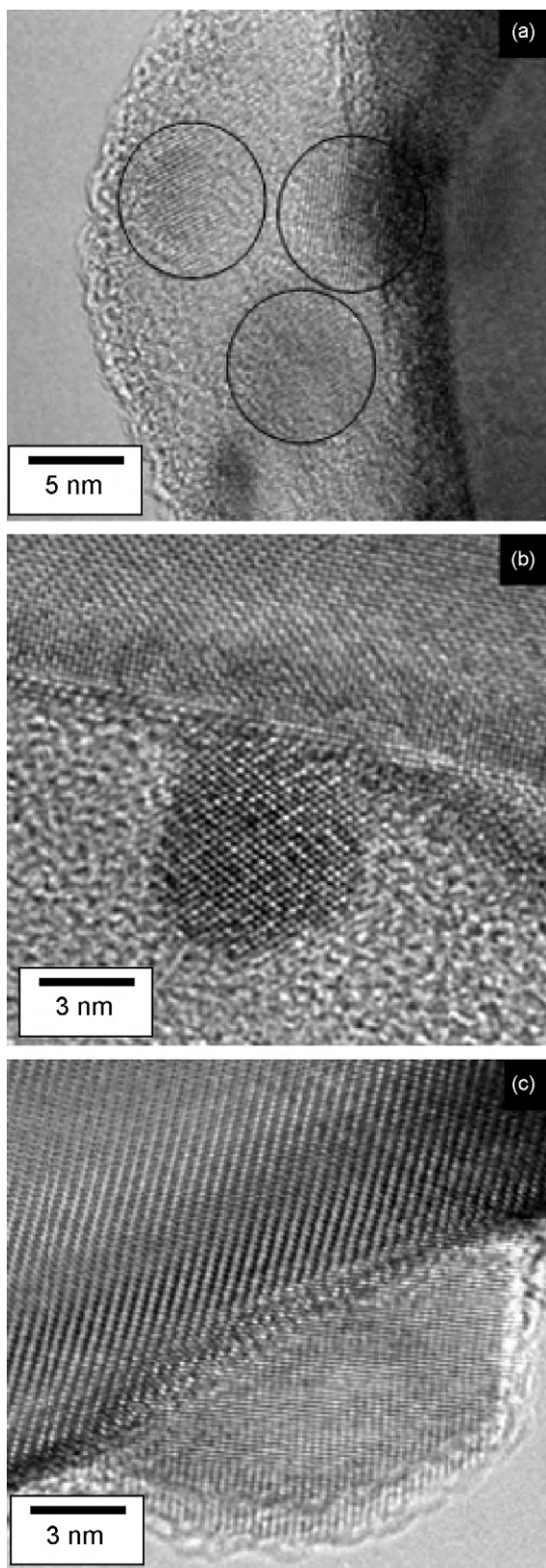


Fig. 8. HRTEM images of the 95 vol% alumina–5 vol% zirconia powder calcined at (a) 500 °C for 1 h (black circles point out zirconia crystallites), (b) 600 °C for 1 h, (c) 1000 °C for 1 h.

tions clearly supported the homogeneous nucleation of zirconia crystallites into the amorphous phase, yielded by the precursor decomposition. Fig. 8b and c gives an overview of the evolution of the contact angle of zirconia nano-crystallites and alumina grains as a function of temperature, precisely after calcination at 600 °C (Fig. 8b) and 1000 °C (Fig. 8c) for 1 h, and of the related, progressive disappearance of the amorphous layer. It can be qualitatively observed that the contact angle decreases with the increase of the calcination temperature, and finally the surface adhesion of zirconia crystals to the alumina grains is observed at the higher treatment temperature.

To improve the information on the evolution of zirconia crystallites, the size distribution of zirconia crystallites after the different heat treatments (temperature range: 500–1000 °C, heating rate of 10 °C min<sup>-1</sup>, soaking time of 1 h) were determined from DF and ADF TEM images (see examples in Fig. 9). The mean zirconia crystallite sizes are 9 nm, 11 nm, 17 nm and 25 nm for the samples treated at 500 °C, 600 °C, 800 °C and 1000 °C respectively, in agreement with the above reported data.

Phase identification was carried out by Raman spectroscopy, since this technique is preferable to investigate the primary crystallization and possible phase transformation in our system, being more sensitive to intermediate-range order, while the phase detectable by XRD must have a periodicity over a length of 5 nm.<sup>22</sup> The analyses were performed on both pure alumina samples and modified powders after *in situ* treatments at 500 °C, 600 °C, 800 °C, 1000 °C and 1200 °C in XRD apparatus (Fig. 10). Raman spectrum of the alumina powder presents several peaks at 378 cm<sup>-1</sup>, 416 cm<sup>-1</sup>, 429 cm<sup>-1</sup>, 451 cm<sup>-1</sup>, 576 cm<sup>-1</sup>, 644 cm<sup>-1</sup> and 750 cm<sup>-1</sup>, in good agreement with the literature.<sup>23</sup> In the spectra of the composite powder others peaks at 144 cm<sup>-1</sup>, 268 cm<sup>-1</sup>, 314 cm<sup>-1</sup>, 458 cm<sup>-1</sup> and 599 cm<sup>-1</sup> appear, which are imputable to zirconia tetragonal structure.<sup>24</sup> No characteristic peaks of the monoclinic<sup>25</sup> or the cubic structure<sup>26</sup> are observed even after treatment at 1200 °C. In both XRD pattern and Raman spectrum of the composite sample calcined at 1200 °C for 12 h only tetragonal zirconia is detectable, confirming that, thanks to its very small crystallite size, tetragonal structure is preserved even after prolonged high-temperature treatments.

#### 4. Discussion: a possible scenario of crystallization process

From the above results, several considerations on the mechanism of zirconia crystallization onto alumina grains surface can be pointed out.

As often mentioned in the literature, the first phase to crystallise from an amorphous zirconium oxide precursor<sup>22,27–30</sup> is usually tetragonal zirconia. Here we show that tetragonal zirconia is present at room temperature after the thermal treatments, even if monoclinic phase is the thermodynamically stable one. Garvie<sup>28</sup> suggested that, for very small crystals, the tetragonal phase could be stable thanks to the smaller surface energy, and he found that when zirconium oxide samples, obtained by precipitation, were heated, the tetragonal crystallites grew to a maximum of 30 nm, before a complete transformation to the monoclinic

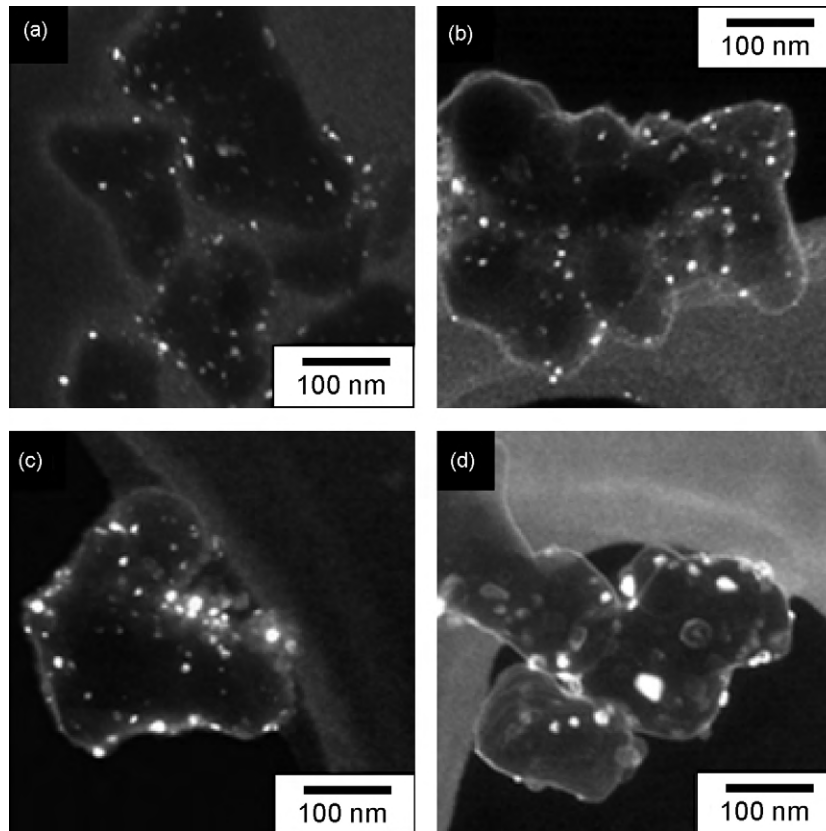


Fig. 9. DF TEM images of 95 vol% alumina–5 vol% zirconia powder after treatments at different temperatures and times: (a) 500 °C – 1 h, (b) 600 °C – 1 h, (c) 800 °C – 1 h, (d) 1000 °C – 1 h.

phase. As a consequence, a critical size for transformation,  $D_c$ , can be calculated, on the basis of the surface free energy for the two phases. The surface free energy of tetragonal nanoparticles depends on several factors, for example on the state of aggregation. Rezaei et al.<sup>29</sup> calculated a  $D_c$  of about 9 nm, for isolated spherical zirconia particles and of 33 nm, when zirconia is within aggregates. In our system, zirconia crystals remained tetragonal in all the samples calcined even at high-temperature for long time (1200 °C for 12 h), and they reached a maximum size of about 32 nm. It is therefore probable that the interface energy between  $\alpha$ -alumina and tetragonal zirconia contributes to lower the total free energy of tetragonal phase respect to the monoclinic one, hindering the related transformation.

Tetragonal zirconia starts to crystallise at very low temperature (about 500 °C), as stated by XRD and TEM investigations. By TEM it was also shown that zirconia crystallites start to nucleate into the amorphous layer upon the alumina grains, yielded by the thermal decomposition of the zirconia precursor, suggesting a mechanism of homogeneous nucleation. Only improving the treatment temperatures, due to the progressive disappearance of the residual amorphous phase, the zirconia crystals approach the alumina grains surface and a related evolution of the contact angle between the two phases is observed.

A very short induction time for crystallization is observed only in the case of isotherm at 500 °C, supporting the hypothesis of a very fast nucleation. Instead, considering the evolution of crystal size as a function of temperature and time, a very slow

crystal growth is determined in the medium–low temperature regimes even for long treatment times, whereas an appreciable increase of the mean zirconia dimension during isothermal treatments starts only above 1000 °C.

The calculated Avrami exponents for isothermal and isochronal treatments are low (<0.5). These values are in agree-

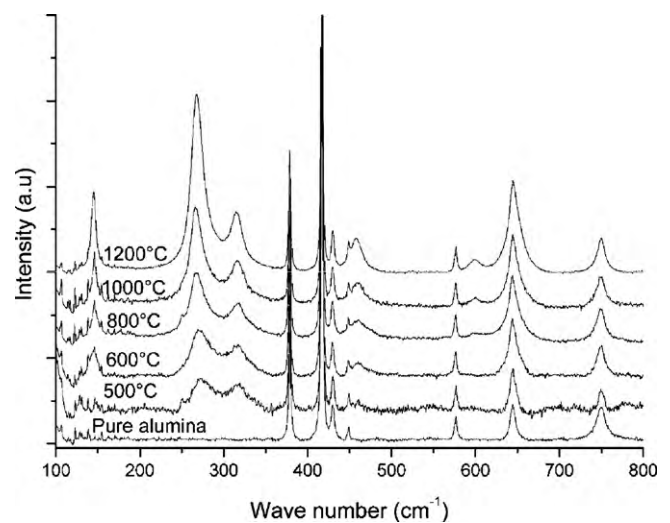


Fig. 10. Raman spectra of pure alumina and 95 vol% alumina–5 vol% zirconia powders after *in situ* treatments in the HT-XR Diffractometer at 500 °C, 600 °C, 800 °C, 1000 °C and 1200 °C.

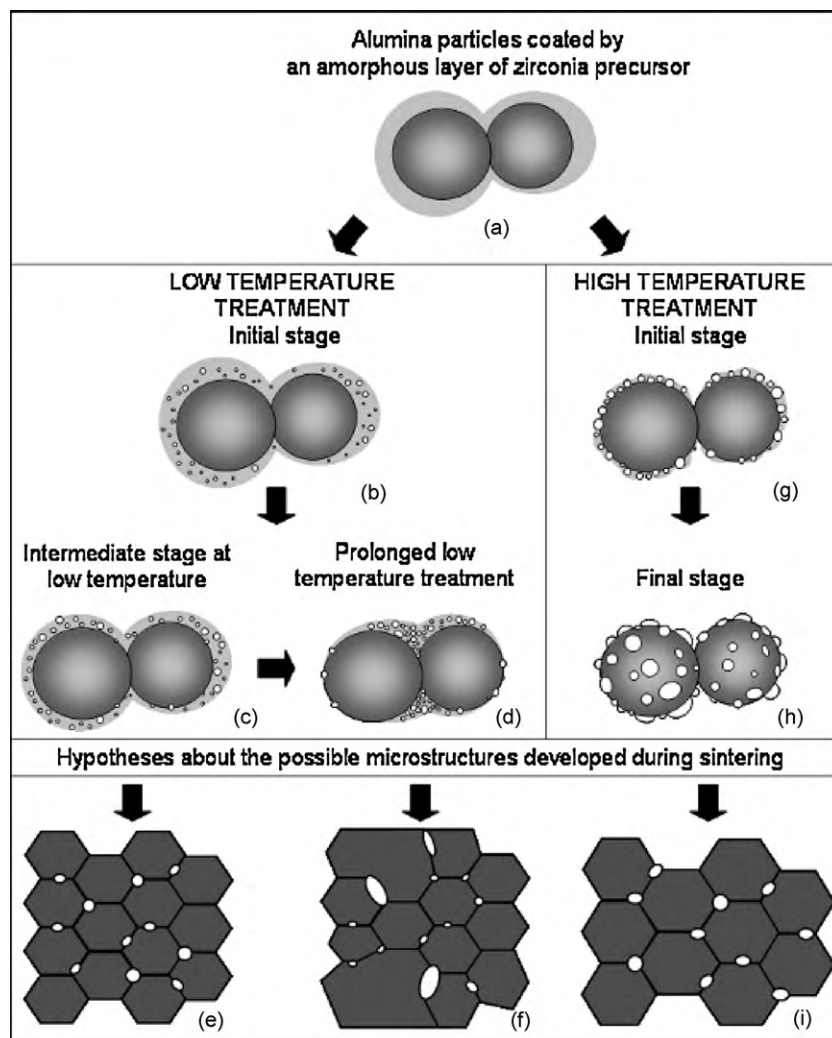


Fig. 11. Possible zirconia crystallization mechanism.

ment with the work of Ghosh et al.,<sup>20</sup> who explained their results by the dominance of interfacial control mechanism over the bulk diffusion in the growth behavior of zirconia. The crystallization from amorphous zirconia as a diffusionless transformation has been already reported in previous studies,<sup>27,28</sup> based on the investigation of the structure of amorphous hydrous  $ZrO_2$ . In the above studies, they described the structure of the amorphous zirconia as made of alternated layers of zirconium and oxygen atoms, with interatomic distances similar to that of tetragonal zirconia. Moreover, by electron diffraction patterns, they claimed that amorphous zirconia seemed to be a bulk sample of crystals nuclei with a structure very close to that of tetragonal phase, but with very short periodicity.<sup>27</sup> The hypothesis of these authors<sup>27,28</sup> can therefore account for a very fast nucleation, as also proposed in the present study, in agreement with the homogeneous nucleation here observed by TEM.

Therefore, the low value of the Avrami exponent could be explained, by analysing the contribution of both nucleation and growth. The nucleation rate cannot be supposed constant: in fact, it is very high at the beginning of the transformation, at temperatures lower than 600 °C, and it becomes moderate by increasing

the treatment temperature. On the contrary, the growth rate is supposed to be low at the temperatures below 1000 °C, due to a poor diffusion rate.

A possible scenario for the zirconia crystallization can be proposed starting from the collected results. After drying the modified powders are made of alumina grains coated with a layer of amorphous zirconia precursor (Fig. 11a). Crystallization is then promoted by thermal treatments; by calcination at low temperature, a homogeneous nucleation of zirconia nanocrystals in the amorphous layer is already observed in the initial stage of the thermal treatment (Fig. 11b), while their growth rate is very slow, so that, at the intermediate stage, a slightly decrease of amorphous phase is observed, mainly imputable to continuous nucleation (Fig. 11c). However, prolonging the treatment at low temperature, the amorphous phase, even if still present, is preferentially drained into discrete pockets among the alumina particles, to reduce the related contact surface (Fig. 11d). Consequently, we hypothesize that the calcination time at low temperature could have a dramatic effect on the final microstructure after sintering. In a first case, the powder calcined for short time contains uniformly distributed zirconia nuclei (Fig. 11c),

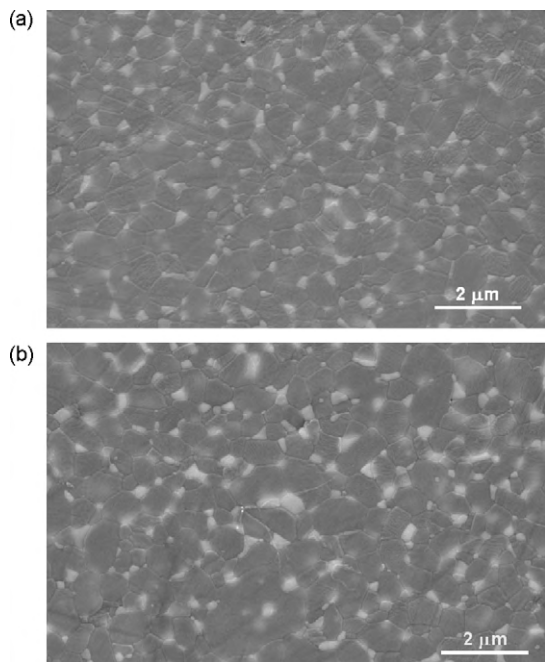


Fig. 12. SEM images of sintered samples obtained from powder previously calcined at 600 °C for 1 h (a) and for 10 h (b).

so that, the resulting microstructure is homogeneous and a narrow size distribution of zirconia grains is obtained (Fig. 11e). Otherwise, the powder calcined at low temperature for longer time contains zirconia nuclei preferentially located into pockets among the alumina particles where the amorphous phase is placed, and few isolated zirconia nano-grains (Fig. 11d). This non-uniform morphology of the composite powder could reasonably give rise to an inhomogeneous microstructure in the sintered materials, where a bimodal distribution size of zirconia grains could be expected, being the larger grains originated by the coalescence of the close nuclei into pockets and the smaller ones by the isolated grains, and also abnormal grain growth could occur into the alumina matrix (Fig. 11f).

Instead, treating at high-temperature, a faster crystallization takes place (Fig. 11g), the amorphous phase disappears at shorter times, comparing with the low temperature treatments, and crystal growth prevails over nucleation, so that larger zirconia crystals are yielded, homogeneously distributed onto the surface of the alumina particles (Fig. 11h). In this case, the hypothesized microstructure of sintered bodies could be homogeneous (Fig. 11i), because the starting composite powder contains uniformly distributed zirconia on the alumina particles surface, but the mean grain size, both for the matrix and the second-phase, is expected to be greater than in the case of materials obtained from the powder treated at low temperature for short time.

A preliminary investigation was carried out in order to support the hypothesized relationship between powder thermal treatment and final microstructure in sintered bodies, as explained in the previously depicted scenario. For this purpose we observed the microstructures of sintered samples, obtained by composite powders treated at 600 °C for 1 h and 10 h, respectively (see Fig. 12a and b).

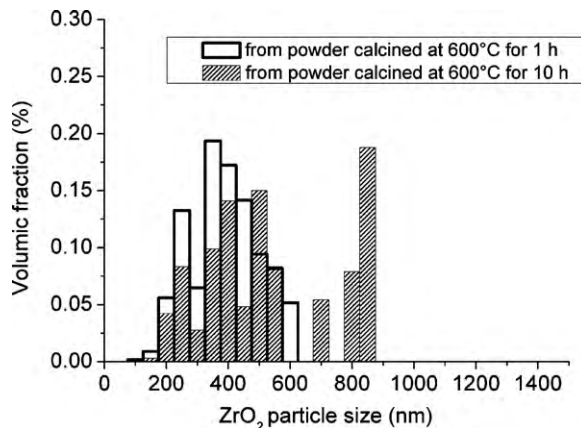


Fig. 13. Zirconia grain size distribution in sintered samples obtained from powder previously calcined at 600 °C for 1 h (a) and for 10 h (b).

A preliminary evidence of a finer and more homogeneous microstructure was found in the case of sintered materials obtained by powders calcined for 1 h. This is even clearer in Fig. 13, where the zirconia grain size distribution is given for the two sintered samples. In agreement with our hypotheses, in the samples obtained by powder calcined for a longer time the zirconia grains distribution is more heterogeneous, and the microstructure resulted coarser.

## 5. Conclusions

The zirconia crystallization mechanism and kinetics were investigated in a composite system, made of  $\alpha$ -alumina particles coated by an amorphous layer of zirconia precursor, obtained by performing a surface modification procedure. TEM observations gave evidence that zirconia starts to crystallize into the amorphous film by homogeneous nucleation, which can be induced by the similarity between the amorphous phase and tetragonal phase, as already stated in literature. The crystallization mechanism can be summarized as follows:

- at low temperature, a fast nucleation from the amorphous layer occurs as the organic by-products start to decompose, while crystal growth is negligible, being the atomic diffusion hindered;
- at higher temperature, the nucleation rate decreases, while diffusion becomes more effective and the growth of the existing nuclei is predominant.

In view of preserving nano-zirconia grains homogeneously dispersed into the  $\alpha$ -alumina matrix, suitable temperature and time of thermal treatment must be carefully selected, being pivotal tools for the tailoring of the powder as well as of the final composite material microstructures. Treatments at low temperature promote the formation of small zirconia crystals (for instance, of 10–15 nm in size at 600 °C), but very long times are needed to achieve a fully crystallization. At the same time, the amorphous layer tends to drain into discrete pockets among the alumina grains, dragging the zirconia crystals. Such gathering of zirconia nanocrystals could promote their coalescence

and growth during sintering, hindering a successful control of the nanostructure. This scenario was confirmed by preliminary observations of the microstructure in sintered bodies, obtained by powders calcined at 600 °C for 1 h and 10 h. However, a deeper investigation on the relationship between the above evolution at the nanoscale and the microstructural development during sintering is now in progress.

Instead, a treatment at higher temperature for a short time promotes a fast disappearance of the amorphous phase layer and the crystallization of larger zirconia grains.

The surface modification techniques, as the simple one described in this paper, are very promising procedures to obtain nanoscaled second-phase grains into a selected matrix, but a deep knowledge of the nucleation and growth steps is required as a robust background of a nanopowder engineering approach in order to achieve the full control of the powder features and, consequently, of the final dense microstructure.

### Acknowledgments

The authors would like to thank G. Montagnac (Ecole Normale Supérieure de Lyon, France) for its support for the Raman spectroscopy experiments and S. Cardinal for HT-XRD. The CLYM (Centre Lyonnais de Microscopie) is gratefully acknowledged for the access to the transmission electron microscope.

The authors thank the European Commission for supporting this work in the framework of Integrated Project “NANOKER-Structural Ceramic Nanocomposites for top-end Functional Applications”, contract no: NMP3-CT-2005-515784.

### References

- Kerkwijk B, Winnubst AJA, Verweij H, Mulder EJ, Metselaar HSC, Schipper DJ. Tribological properties of nanoscale alumina–zirconia composite. *Wear* 1999;**225–229**:1293–302.
- Gutknecht D, Chevalier J, Garnier V, Fantozzi G. Key role of processing to avoid low temperature ageing in alumina zirconia composites for orthopaedic application. *J Eur Ceram Soc* 2007;**27**:1547–52.
- Rahaman MN, Yao A, Sonny Bal B, Garino JP, Ries MD. Ceramics for prosthetic hip and knee joint replacement. *J Am Ceram Soc* 2007;**90**(7):1956–88.
- Srdic VV, Radonjic L. Transformation toughening in sol–gel-derived alumina–zirconia composites. *J Am Ceram Soc* 1997;**80**(8):2056–60.
- Freim J, McKittrick J. Modeling and fabrication of fine-grain alumina–zirconia composites produced from nanocrystalline precursors. *J Am Ceram Soc* 1998;**81**(7):1773–80.
- Hannink RHJ, Kelly PM, Muddle BC. Transformation toughening in zirconia-containing ceramics. *J Am Ceram Soc* 2000;**83**(3):461–87.
- Tuan WH, Chen RZ, Wang TC, Cheng CH, Kuo PS. Mechanical properties of Al<sub>2</sub>O<sub>3</sub>/ZrO<sub>2</sub> composites. *J Eur Ceram Soc* 2002;**22**:2827–33.
- De Aza AH, Chevalier J, Fantozzi G, Schehl M, Torrecillas R. Crack growth resistance of alumina, zirconia and zirconia toughened alumina ceramics for joint prostheses. *Biomaterials* 2002;**23**:937–45.
- Sarkar D, Mohapatra D, Ray S, Bhattacharyya S, Adak S, Mitra N. Nanostructured Al<sub>2</sub>O<sub>3</sub>–ZrO<sub>2</sub> composite synthesized by sol–gel technique: powder processing and microstructure. *J Mater Sci* 2007;**42**:1847–55.
- Jayaseelan D, Nishikawa T, Awaji H, Gnanam FD. Pressureless sintering of sol–gel derived alumina–zirconia composites. *Mater Sci Eng A* 1998;**A256**:265–70.
- Upadhyaya DD, Gonal MR, Prasad R. Studies on crystallization behaviour of 3Y-TZP/Al<sub>2</sub>O<sub>3</sub> composite powders. *Mater Sci Eng A* 1999;**A270**:133–6.
- Kikkawa S, Kijima A, Hirota K, Yamaguchi O. Soft solution preparation methods in a ZrO<sub>2</sub>–Al<sub>2</sub>O<sub>3</sub> binary system. *Solid State Ionics* 2002;**151**:359–64.
- Chandradass J, Yoon JH, Bae D. Synthesis and characterization of zirconia doped alumina nanopowder by citrate-nitrate process. *Mater Sci Eng A* 2008;**A473**:360–4.
- Schehl M, Diaz JA, Torrecillas R. Alumina nanocomposites from powder–alkoxide mixtures. *Acta Mater* 2002;**50**:1125–39.
- Palmero P, Naglieri V, Chevalier J, Fantozzi G, Montanaro L. Alumina-based nanocomposites obtained by doping with inorganic salt solution: application to immiscible and reactive system. *J Eur Ceram Soc* 2009;**29**:59–66.
- Kim DJ, Jang JW, Lee HL. Effect of tetravalent dopants on Raman spectra of tetragonal zirconia. *J Am Ceram Soc* 1997;**80**(6):1453–61.
- Petrova N, Todorovsky D. Thermal decomposition of zirconium–yttrium citric complexes prepared in ethylene glycol and water media. *Mater Res Bull* 2006;**41**:576–89.
- Avrami M. Kinetics of phase change. *J Chem Phys* 1939;**7**:1103–12.
- Clupper DC, Hench LL. Crystallization kinetics of tape cast bioactive glass 45S5J. *Non-Cryst Solids* 2003;**318**:43–8.
- Ghosh A, Upadhyaya DD, Prasad R. Crystallization behavior of ZrO<sub>2</sub>–Y<sub>2</sub>O<sub>3</sub> powders: in situ hot-stage XRD technique. *J Am Ceram Soc* 2002;**85**(10):2399–403.
- Chen SG, Yin YS, Wang DP, Li J. Reduced activation energy and crystalline size for yttria-stabilized zirconia nano-crystals: an experimental and theoretical study. *J Cryst Growth* 2004;**267**:100–9.
- Keramidas VG, White WB. Raman scattering study of the crystallization and phase transformations of ZrO<sub>2</sub>. *J Am Ceram Soc* 1974;**57**(1):22–4.
- Richet P, Gillet P, Pierre A, Bouhifd MA, Daniel I, Fiquet G. Raman spectroscopy, X-ray diffraction, and phase relationship determinations with a versatile heating cell for measurements up to 3600 K (or 2700 K in air). *J Appl Phys* 1993;**74**(9):5451–6.
- Bouvier P, Lucazeau G. Raman spectra and vibrational analysis of nanometric tetragonal zirconia under high pressure. *J Phys Chem Solids* 2000;**61**:569–78.
- Kim B, Hahn J, Han KR. Quantitative phase analysis in tetragonal-rich tetragonal/monoclinic two phase zirconia by Raman spectroscopy. *J Mater Sci Lett* 1997;**16**:669–71.
- Phillippe CM, Mazdiyasn KS. Infrared and Raman spectra of zirconia polymorphs. *J Am Ceram Soc* 1971;**54**(5):254–8.
- Livage J, Doi K, Mazieres C. Nature and thermal evolution of amorphous hydrated zirconium oxide. *J Am Ceram Soc* 1968;**51**(6):349–53.
- Garvie R. The occurrence of metastable tetragonal zirconia as crystallite size effect. *J Phys Chem* 1965;**69**(4):1238–43.
- Rezaei M, Alavi SM, Sahebdehfar S, Yan Z, Teunissen H, Jacobsen JH. Synthesis of pure tetragonal zirconium oxide with high surface area. *J Mater Sci* 2007;**42**:1228–37.
- Molodetsky I, Navrotsky A, Paskowitz MJ, Leppert VJ, Risbud S. Energetics of X-ray-amorphous zirconia and the role of surface energy in its formation. *J Non-Cryst Solids* 2000;**262**:106–13.